2009 Digital Image Computing: Techniques and Applications

Automatic mass segmentation based on adaptive pyramid and sublevel set analysis

Fei Ma Mariusz Bajger Murk J. Bottema
Flinders University, Adelaide
SA 5001, Australia
feim@csem.flinders.edu.au *

Abstract

A method based on sublevel sets is presented for refining segmentation of screening mammograms. Initial segmentation is provided by an adaptive pyramid (AP) scheme which is viewed as seeding of the final segmentation by sublevel sets. Performance is tested with and without prior anisotropic smoothing and is compared to refinement based on component merging. The combination of anisotropic smoothing, AP segmentation and sublevel refinement is found to outperform other combinations.

1 Introduction

In many applications of mammography, segmentation of regions of interest (ROI) is one of the essential steps. However, isolation of ROIs in mammography has proved not to be an easy task. Difficulties in mammogram segmentation stem from the complexity of the breast itself and the nature of the mammogram, which is a 2D projection of a 3D object. Masses in breasts are normally surrounded with various types of tissue with different densities, and thus usually depict themselves without clear boundaries in the corresponding mammograms. The difficulty of segmentation in mammography is further compounded by the noise inevitably introduced during the image acquisition process.

Medical image segmentation based on level sets has been studied in the literature [9, 3, 2] and has been shown capable of segmenting ROIs (In literature, different names were used. A discussion on this is presented in Section 3.1). An important step in the level sets based segmentation is identification of the correct level within the sets that best describe a salient region. [9] used the isolabel contour to describe the problem. In that method, the shapes of successive contours were matched by comparing sequences of turning-angles that were extracted from the corresponding contours. A contour that had a large shape change compared with the next contour was identified as the contour of a salient region. The method was evaluated on 75 computed-tomography angiography (CTA) data and results obtained by the method were compared to the results manually edited by experts. The evaluation results verified a null hypothesis that the difference between the results obtained by the method and the experts was not significantly different to the difference between the results obtained by different experts. In [3], iso-level contours were extracted for the entire image. An inclusion tree was introduced to organize the iso-level contours and a minimum nesting depth was used to extract the salient regions. The method was tested on a set of 48 mammograms and 46 masses were correctly extracted. However, accuracy of the extraction was not evaluated. [2] first detected seeds from mammograms, and then extracted concentric layers for each seeds based on the distance between the centroids of consecutive layers. The method was evaluated on multiple sets of mammograms and sensitivities and detection rates were analyzed.

In this paper, we present a method based on the adaptive pyramid (AP) segmentation and sublevel set analysis. The graph based AP segmentation algorithm was used in several applications in mammogram analysis and produced good results [7, 5]. Although AP has been found robust in segmenting salient objects [6] and effective in isolating the ROI with respect to the number of true masses to be segmented, in our current implementation, we found that the boundaries of the ROIs obtained by AP were generally not accurate. The components obtained by the AP were generally within the ROIs. The boundaries of masses are important because both local properties of boundaries such as spiculation or smoothness as well as global properties such as oval shapes or lobular shapes are used to distinguish malignant and benign masses. In this study, the AP segmented components were used as initial seeds and the sublevel set analysis was applied on these components. Sublevel sets analysis with initial seeds avoids the difficulty of identifying correct levels that best describe the suspicious regions

*This work was supported by NBCF

978-0-7695-3866-2/09 $26.00 © 2009 Crown Copyright
DOI 10.1109/DICTA.2009.47

globally. An inclusion tree and minimum nesting depth [3] were also used. In contrast to [3], in this study, the maximum of the minimum nesting depth is found insufficient to locate the correct sublevel set. Instead, we found that the minimum nesting depth of the best contour is always a local maximum among the minimum nesting depths of the sublevel sets. This knowledge was used together with an $AreaRatio$ to locate the best set.

This paper is organized as follows. Section 2 briefly describes the AP algorithm. Section 3 introduces the sublevel sets, the inclusion tree and minimum nesting depth. The detailed implementation of the method is presented in Section 4. Section 5 describes experiments that we conducted to evaluate the proposed method. Discussion and conclusion are provided in Section 6.

2 Segmentation by adaptive pyramid (AP)

The graph based AP algorithm was implemented in our study to segment mammograms. The details of this algorithm and the tuning up for mammogram segmentation can be found in [7]. One advantage of using the AP algorithm was the capability of combining both local and global information. Compared with other graph theoretic segmentation methods that are prohibitively slow for the current application, the AP method gives a reasonable balance between the performance and speed.

3 Sublevel set map

3.1 Sublevel set

Mammograms are complex images. Mass regions in a mammogram are normally not accompanied with clear boundaries. However, mass regions often yield a pattern of concentric rings with gradually declining intensities when moving from the inner to the outer ring. In [2], within a total number of 281 malignant masses analyzed, 96% of masses were found having multiple concentric rings. Only 7 of these 281 masses had concentric rings fewer than 3 concentric rings.

Multilevel thresholding of a suspicious region with a fine partition of intensity splits the region into a set of rings. Pixels that lie in the same ring are in the same intensity level. The set of pixels that lie within a level comprise a *sublevel set*. More formally, let I be the intensity range of a mammogram, a partition of the intensity range is $I(P) = \{i_j | j = 1 \dots t \quad \text{and} \quad i_{min} = i_1 < i_2 < i_3 < \dots < i_t = i_{max}\}$, here i_{min} and i_{max} are the minimum and maximum value within intensity range I. A sublevel set $C_R(i)$ for a given intensity level i and a given ROI R is given by:

$$C_R(i) = \{(x, y) | (x, y) \in R \ \text{ and } \ I(x, y) \geq i\}.$$

The collection of sublevel sets of R is referred to as a sublevel set map $CM(R)$ for R, and is given by:

$$CM(R) = \{C_R(i_j) | i_j \in I(P), j = t_1, \dots, t_n\}.$$

In the literature, other names have been used to describe the sublevel set, such as isolabel contour in [9], iso-level contour [3] and concentric layers [2]. The different names indicate different approaches. In [9], the name isolabel contour is used because the method presented in that paper extracted and compared the contours and also used the labels to mark the contours. [3] used the term iso-level contour as that study also focused on the contour formed by the pixels in the same intensity level. Concentric layers used in [2] had the same definition as the sublevel set used in this paper. That method used the concentric properties between the layers. In the method presented in this paper, the analysis is based on the set of pixels which has exactly the same definition as the mathematical term sublevel set.

3.2 Inclusion tree

The entire pattern of the sublevel sets in a sublevel set map can be described as a relationship of enclosure. For two sets $C_R(i_m)$ and $C_R(i_n)$ belonging to the same sublevel set map $CM(R)$, $C_R(i_m)$ is enclosed by $C_R(i_n)$

$$C_R(i_m) \subset C_R(i_n).$$

A sublevel set map can be represented in the form of a rooted tree, with the outermost set as the root and a directed edge connecting $C_R(i_n)$ to $C_R(i_m)$ (from $C_R(i_n)$ to $C_R(i_m)$) if and only if $C_R(i_m) \subset C_R(i_n)$ (see Fig. 1). The node $C_R(i_n)$ is called the parent of node $C_R(i_m)$ and node $C_R(i_m)$ is called the child of node $C_R(i_n)$. Such a rooted tree is called an *inclusion tree*.

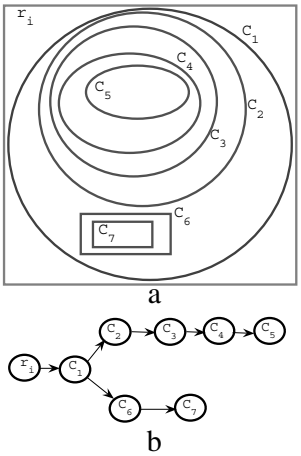

Figure 1: An example of an inclusion tree. A sublevel set map map is shown in (a). (b) shows the corresponding inclusion tree.

A *path* $P(i_1, i_n)$ connecting nodes $C_R(i_1)$ and $C_R(i_n)$ in an inclusion tree is an ordered sequence with no repeated nodes $C_R(i_1), C_R(i_2), \ldots, C_R(i_n)$, such that from each of node $C_R(i_t), t = 1, \ldots, n-1$, there is an edge connecting the next node $C_R(i_{t+1})$ in the sequence. The *length* $L(P(i_1, i_n))$ of the path $P(i_1, i_n)$ is defined as the number of edges in the path. The *degree* $D(C_R(i))$ of a node $C_R(i)$ is defined as the number of children it has. A node whose degree is 0 is called a *leaf*.

3.3 Minimum nesting depth

In a sublevel set map, a *nesting depth* for a sublevel set describes the number of sublevel sets enclosed by this set. More formally, the nesting depth of a node $C_R(i_n)$ with respect to a leaf node $C_R(i_m)$ is the length of path $P(i_n, i_m)$. A set may nest several leaves, for example in Figure 1, leaves C_5 and C_7 are both nested by C_1. In this case, the minimum of the nesting depths of the set $C_R(i)$ to all its leaves is defined as the minimum nesting depth $\gamma(C_R(i))$, which is given by:

$$\gamma(C_R(i)) = \min_t L(P(i, t)),$$

for any leaf $C_R(t)$ nested within $C_R(i)$.

Mass regions normally yield a conspicuous pattern of multilevel rings. The γ of the sublevel set increases when moving from the center toward the boundary of the mass. When moving past the boundary of the mass, the mass merges into the surrounding background. The sublevel set starts to enclose more regions and the corresponding node in the inclusion tree connects to more leaves. In Figure 1, after level C_2, the region starts to merge to the background, and level C_1 contains another leaf C_7. The minimum nesting depth $\gamma(C_1) = 2$ is smaller than $\gamma(C_2) = 3$. γ of the sublevel set can be a useful tool in analyzing the inclusion tree for the purpose of identifying the best sublevel that best describes a suspicious region.

4 Method

The AP algorithm segments the mammogram into many components [7, 5]. In our current implementation, AP can locate most of the suspicious regions. However, the boundaries of the ROIs obtained by AP were generally not accurate and were generally inside the true boundaries. In this study, the AP segmentation results were used as initial seeds and sublevel sets analysis was applied on these seeds to refine the boundaries of the corresponding regions.

The first step in the process is an anisotropic diffusion. Some noise is inevitably introduced during the acquisition of the mammogram. The existence of the noise may cause sublevel sets separated or jagged. An anisotropy diffusion filter based on Perona and Malik's work [8] is used to remove the noise and at the same time to enhance the edges.

4.1 Extraction of sublevel sets

Before the extraction of the sublevel sets, the anisotropy diffused image is multi-thresholded with a partition of intensity range to produce a set of images. In this study, the images selected for the experiments are rescaled to an intensity range of (0, 255). This intensity range is equally partitioned with a partition interval of every 3 consecutive intensity values. Other partition intervals (interval = 2,4) were also tried but no significant difference on the extracted sublevel sets was observed.

For each intensity level i_j in an intensity partition $I(P)$, an image is produced by retaining pixels in the anisotropy diffused image whose intensities are greater than or equal to i_j. This image is labeled as i_j.

A recursive procedure is then used to extract the sublevel sets of a region. At the beginning, the procedure requires two parameters: a current set $C(i_j)$ and a current label i_j. During the process, single isolated components within the set $C(i_j)$ in the thresholded image i_{j+1} are located. The corresponding pixel sets of the located components are added to the inclusion tree by adding children nodes to the node $C(i_j)$. The procedure then recursively extracts sublevel sets for each isolated component together with the intensity level i_{j+1}.

4.2 Exclusion of non-interest components

When put together, all components obtained from AP segmentation cover the whole breast. Not all components are of interest. For example, components belonging to the background region and with low intensity contrast have low probabilities of being masses. Inclusion of these components increases the processing time, and may also negatively affect the extraction of boundaries of the true masses.

Before the process of sublevel set analysis, a simple procedure is used to determine if the process needs to be performed. The procedure extracts the sublevel set map within a component and counts the leaves in the corresponding inclusion tree. If the inclusion tree has more than 4 leaves, the component is considered as not sufficiently homogeneous and is excluded for further analysis.

4.3 Backward extraction

Boundaries of the AP segmented components tend to be within the true boundaries of the ROIs. Sublevel set analysis based on these components will not lead to improvements on the boundaries. To include the true boundary into the analysis region, the component need to be expanded.

The procedure used to expand the component is also based on the sublevel set analysis. It is similar to the recursive procedure introduced in Section 4.1. It also accepts two parameters, a current set $C(i_j)$ and a current label i_j. However, instead of locating all isolated regions within $C(i_j)$ in the thresholded image i_{j+1}, this expanding procedure locates the region in the image i_{j-1} which contains $C(i_j)$. The extracted region $C(i_{j-1})$ in image i_{j-1} is then taken as current set and the procedure continues to extract the next sublevel set $C(i_{j-2})$ based on the current $C(i_{j-1})$ and the current label i_{j-1}. A condition, $AreaRatio$, is used to stop the process. The $AreaRatio$ is defined as

$$AreaRatio = \frac{|C(i_{j-1})| - |C(i_j)|}{|C(i_j)|},$$

where $|C(i_j)|$ is the number of pixels contained in the set $C(i_j)$. In this study, $AreaRatio > 1.0$ is found sufficient to stop the procedure.

Comparing to the recursive procedure used in the Section 4.1, the expanding procedure extracts sublevel sets backwardly, and so is called *backward extraction*. The procedure introduced in Section 4.1 is called *forward extraction*.

4.4 Best contour identification

The $AreaRatio$ is only a raw condition, it is not expected to stop the expanding procedure right on the true boundary of a ROI. The best sublevel set is identified based on the analysis to the sublevel set map and the inclusion tree of the expanded component.

To locate the sublevel set in the inclusion tree that best describes the suspicious region, a set $C(i_{ori})$ which best fit the original component is firstly located in the inclusion tree. As raw AP segmented component is generally inside the real boundary of the corresponding ROI, the node of the best sublevel set is in the path from the root $C(i_{min})$ to $C(i_{ori})$, $P(i_{min}, i_{ori}) = [C(i_{min}), C(i_1), C(i_2), \ldots, C(i_t), C(i_{ori})]$.

Extraction of the boundary of the mass region is an ill-defined problem, as masses in the breasts intersect with surrounding tissues and normally project no clear boundaries in the mammogram. However, for the purpose of the computer-aided diagnosis (CAD), it is necessary to define a boundary for a mass like region. In our experiments, we observed that the γ of the best sublevel set is normally a local maximum within the γs of the nodes in the path $P(i_{min}, i_{ori})$.

The $AreaRatio$ is also used in selecting the best sublevel set in $P(i_{ori}, i_{min})$. In this study, $AreaRatio > 0.31$ is set empirically. If the $AreaRatio$ between $C(i_m)$ and $C(i_{m-1})$ is larger than 0.31, then all nodes from $C(i_{m-1})$ to the root $C(i_{min})$ in $P(i_{min}, i_{ori})$ are rejected as candidate nodes.

The final selection of the candidate set is, within all nodes in $P(i_{min}, i_{ori})$ whose γs are local maximum and who meet the $AreaRatio$ condition, the node having maximum γ is selected as the best sublevel set.

5 Experiments

174 mammograms from a local archive were used in this paper for the evaluation. The set included both mediolateral oblique (MLO) view and cranial-caudal (CC) view mammograms (94 MLO and 80 CC). 43 images contained malignant masses that were confirmed by histopathology.

All images were digitized using a Vidar Diagnostic Pro Advantage digitizer (48 μm spatial resolution and 12 bit depth). Images are originally 5296×3478 pixels in size. For processing, images were downsampled by a factor of $8 \times 8 \rightarrow 1$. The intensity range of the images is also rescaled to an intensity range of (0, 255) for the convenience of processing.

The performance of the proposed method was evaluated in two ways. First, the results produced by the method were compared to manually annotated results. Second, a mass classification schema was applied on the segmentation results to measure the performance of the proposed method on mass classification.

For comparison, the results obtained by the proposed method are compared to the results obtained from AP segmentation, the results obtained by a merging process applied on the AP segmented components, and the results obtained by using the same proposed method but without the anisotropy diffusion. The merging process was previously developed to merge over-segmented components after AP segmentation [5].

In the following sections, "AP" refers to the results obtained directly after AP segmentation, "Mg" refers to the results by merging process, "Sls" refers to the results by the proposed method and "Sls*" refers to the results obtained using the same method but without anisotropy diffusion.

A. Comparison to manual annotation

The goal of this experiment was to quantitatively measure the performance of the proposed method by comparing the segmentation results with manually drawn results. For this purpose, 37 images with malignant masses were selected from the data set to use in this experiment. The images were previously annotated by a radiologist with locations of the malignant masses indicated with boxes. The box covered the whole mass and the coordinates of two diagonal vertices were recorded and kept in the file. The selection of the 37 images was based on two conditions, first, the image contained malignant masses that were confirmed by

histopathology, and second, manual annotation was available.

Although the boxes given by the radiologist covered the whole malignant mass, the boundary of the box did not meet the true boundary of the mass and normally contained extra space. To be able to quantitatively and accurately measure the performance, boundaries of the malignant masses in the selected 37 images were manually drawn independently by two authors using an open-source image analysis toolkit (ImageJ, [1]). The union of the two annotated areas was used as the true area of the mass.

A measure, $\mathcal{R}$, further called the mass coverage ratio, commonly used in literature (see e.g. [4]), was used to measure how well the boundaries of the segmented components meet the manually drawn true boundaries. The mass coverage ratio was computed for each component and each segmentation. It is defined by

$$\mathcal{R} = \frac{|C \cap T|}{|C \cup T|}, \tag{1}$$

where C is a segmented component, T is the manually drawn region and $|C|$ is the area of component C.

Fig. 2 shows a plot of the fraction of malignant masses correctly segmented at various coverage ratio levels for all images. The graph shows that the proposed method performed best. The Sls* performed better than the AP segmentation and merging.

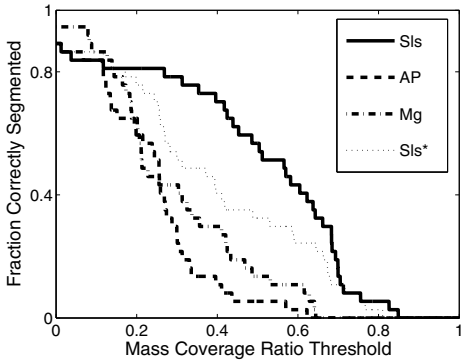

Figure 2: The performance of 4 methods as compared with manually drawn boundaries.

B. Performance on mass classification

The manually drawn boundaries provided quantitative measurements to the accuracy of the segmentation. However, masses in the breast intersect with surrounding tissues and normally project no clear boundaries in the mammogram. The purpose of this study is to develop a mass isolation method to serve in the research toward analysis of temporal mammograms. A better way to evaluate the proposed method is to evaluate the performance of the method under a mass detection schema. In this section, a mass classification schema was applied on the obtained results. In the mass classification schema, a set of 17 standard features similar to those in [5] were used to characterize the segmented components.

The k-fold validation with k=7 was used to validate the performance of the classification schema on the segmentation results. In this validation method, the set of 174 mammograms were randomly split into 7 complementary subsets. Mammograms containing malignant masses were also randomly evenly distributed into the subsets. Thus, each subset contained 6 malignant masses (the last subset contained 7). Of the 7 subsets, a single subset was retained as the validation set, and the remaining subsets were used as training data. The cross-validation process was then repeated 7 times, with each of the 7 subsets used exactly once as the validation data.

In each round of the cross-validation process, the Fisher Linear Discriminant (LDA) analysis was used to optimize the parameters for the mass classification based on the training set. The performance of the whole detection schema was evaluated using the receiver operating characteristic (ROC) analysis and indicated by the area under the ROC curve (A_z score).

Fig. 3 shows the results of the detection on the Sls, Sls*, Mg and AP. Classification on the Sls components gave the best results with 0.88 of A_z score on training set and 0.87 on the validation data. Segmentation on Sls* results gave the second best performance with 0.85 of A_z score on training data and 0.83 on testing data. The merging process developed previously merges some components based on a series of criteria. The results obtained with merging process showed improvements compared to the AP segmented components. The A_z scores for the training data and the validating data were 0.79 and 0.78, respectively. The AP segmented components gave worst results with 0.78 and 0.74 A_z score for training and validating data respectively.

6 Discussion and conclusion

After the AP segmentation, three malignant masses were already missed. All these three malignant masses in the corresponding images are adjacent to the boundaries of the breast, and are close to the dark background. The intensity contrasts of these three masses are low. The anisotropy diffusion also failed in capturing any signs of these malignant masses. The failure on these three images dramatically decreased the performance of the proposed method. In Fig. 3, the dashed curves in all four images, which were the classification performance on training data, can only reach 0.9, leaving large spaces to the top.

On three images, the segmented mass components exceeded the annotated boxes. In all three cases, better sub-

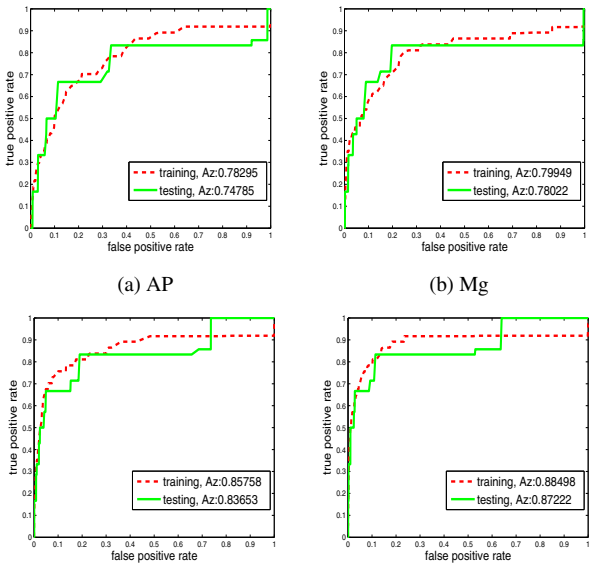

(a) AP (b) Mg

(c) Sls* (d) Sls

Figure 3: Classification results on components obtained by (a) AP, (b) Mg, (c) Sls* and (d) Sls.

level sets exist and their γs are also local maximum. However, the proposed method picked up the wrong sets which have higher γ. The masses in these three cases have no clear boundaries, they merge into the surrounding backgound gradually, thus showing no significant change of area ratio between the consecutive levels.

Fig. 4 shows some examples with masses correctly identified. The last column of Fig. 4 shows a spiculated mass. In this example, the diffused image shows no clear intensity levels around the spiculated mass area and the sublevel set analysis can not improve the boundary for this mass.

The anisotropy diffusion removes the noise in the image and at the same time enhances the strong edges, forming clear pattern of multiple intensity levels around the ROIs. In both [9] and [3], anisotropy diffusion was used to reduce noises and to enhance the image. The application of the proposed method on images without anisotropy diffusion was designed to investigate the impact of the anisotropy diffusion. Results shown in Fig. 2 and 3 show that the proposed method also obtained good results without the anisotropy diffusion, compared to the AP and Mg results.

The purpose of the study reported in this paper was to develop an automatic method to segment ROIs in mammograms. The proposed method used the AP segmentation components as initial seeds and applied the sublevel set analysis to improve the boundaries of components. The experiment showed significant improvements on the mass segmentation both in terms of the accuracy of the segmentation and in terms of the performance on mass detection. In conclusion, the proposed method shows potential in delineating the masses in mammograms.

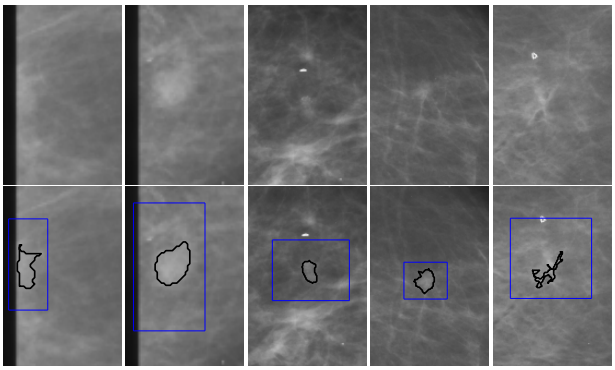

Figure 4: Examples of correctly segmented masses. Top row: original mammograms that include masses. Bottom row: segmented masses were outlined with black boundaries. The boxes were annotated by radiologist.

References

[1] M. D. Abramoff, P. J. Magelhaes, and S. J. Ram. Image processing with imageJ. *Biophotonics Int.*, 11(7):36–42, 2004.

[2] N. H. Eltonsy, G. D. Tourassi, and A. S. Elmaghraby. A concentric morphology model for the detection of masses in mammography. *IEEE Transactions on Medical Imaging*, 26(06):880–889, June 2007.

[3] B.-W. Hong and M. Brady. A topographic representation for mammogram segmentation. In *MICCAI 2003*, Toronto. Canada, 2003. Springer.

[4] M. A. Kupinski and M. L. Giger. Automated seeded lession segmentation on digital mammograms. *IEEE Transactions on Medical Imaging*, 17(4):510–517, 1998.

[5] F. Ma, M. Bajger, and M. J. Bottema. Temporal analysis of mammograms based on graph matching. In *Digital Mammography / IWDM*, pages 158–165, Tucson, AZ, USA, 2008. Springer.

[6] F. Ma, M. Bajger, and M. J. Bottema. Robustness of two methods for segmenting salient features in screening mammograms. In *DICTA 2007*, pages 112–117, Glenelg, South Australia, Dec. 2007. IEEE.

[7] F. Ma, M. Bajger, J. P. Slavotinek, and M. J. Bottema. Two graph theory based methods for identifying the pectoral muscle in mammograms. *Pattern Recognition*, 40:2592–2602, 2007.

[8] P. Perona and J. Malik. Scale-space and edge detection using anisotropic diffusion. *IEEE Trans. Pattern Anal. Machine Intell.*, 12:629–639, July 1990.

[9] S. Shiffman, G. D. Rubin, and S. Napel. Medical image segmentation using analysis of isolable-contour maps. *IEEE Transactions on Medical Imaging*, 19(11):1064–1074, Nov. 2000.